Angular distribution for the elastic scattering of electrons from $Ar^+(3s^2 3p^5\ ^2P)$ above the first inelastic threshold

S. J. Brotton, P. McKenna,* G. Gribakin, and I. D. Williams
School of Mathematics and Physics, The Queen's University of Belfast, Belfast BT7 1NN, United Kingdom
(Received 7 December 2001; published 20 December 2002)

The measured angular differential cross section (DCS) for the elastic scattering of electrons from $Ar^+(3s^2 3p^5\ ^2P)$ at the collision energy of 16 eV is presented. By solving the Hartree-Fock equations, we calculate the corresponding theoretical DCS including the coupling between the orbital angular momenta and spin of the incident electron and those of the target ion and also relaxation effects. Since the collision energy is above one inelastic threshold for the transition $3s^2 3p^5\ ^2P - 3s 3p^6\ ^2S$, we consider the effects on the DCS of inelastic absorption processes and elastic resonances. The measurements deviate significantly from the Rutherford cross section over the full angular range observed, especially in the region of a deep minimum centered at approximately 75°. Our theory and an uncoupled, unrelaxed method using a local, spherically symmetric potential by Manson [Phys. Rev. **182**, 97 (1969)] both reproduce the overall shape of the measured DCS, although the coupled Hartree-Fock approach describes the depth of the minimum more accurately. The minimum is shallower in the present theory owing to our lower average value for the *d*-wave non-Coulomb phase shift σ_2, which is due to the high sensitivity of σ_2 to the different scattering potentials used in the two models. The present measurements and calculations therefore show the importance of including coupling and relaxation effects when accurately modeling electron-ion collisions. The phase shifts obtained by fitting to the measurements are compared with the values of Manson and the present method.

DOI: 10.1103/PhysRevA.66.062706 PACS number(s): 34.80.Kw

I. INTRODUCTION

The angular differential cross section (DCS) for electrons scattered elastically by a bare nucleus is described by the Rutherford formula. If the ion contains electrons, however, the potential departs from the Coulomb form close to the ion, which causes additional non-Coulomb phase shifts relative to the Coulomb phase shifts. The structure produced by the non-Coulomb phase shifts causes deviations from the Rutherford cross section and is highly sensitive to the scattering potential used in the calculations. Electron-ion interactions are consequently more difficult to model theoretically than electron scattering from the corresponding neutral isoelectronic state and, hence, especially careful treatment of the exchange and polarization terms is required [1]. Experiments are therefore required to assess the accuracy of the approximations used in the calculations, and the experimental DCS presented here provides a more stringent test than measurements of the total cross section. The understanding of how electrons and ions interact is required to model high-temperature plasmas, for example, which finds applications in a diverse range of fields including astrophysics, controlled thermonuclear fusion, the physics of the upper atmosphere, and x-ray lasers.

In comparison to the scattering of electrons from neutral atoms, there are few experiments or theoretical calculations for electron-ion collisions. The measurements of the elastic DCS are especially scarce due to their difficulty, which is partly a consequence of the low density of target ions in the beam. There are measurements of the elastic DCS for Xe^{6+}, Xe^{8+}, and Ba^{2+} below 50 eV at scattering angles between 30° and 90° [2], Ar^+ and Kr^+ at 3.3 eV in the angular range of 120° to 170° [3,4], Na^+ [5], Cs^+ [6], Ar^{8+} and Xe^{q+} where $3 \leqslant q \leqslant 6$ in the increased angular range between 32° and 148° and at lower collision energies [7] compared to their earlier measurements [2], N^{q+} with q of 1, 2, and 3 [4,8], and Ar^{7+} and Ar^{8+} [9]. Similar processes occur in fast ion-atom and ion-molecule ionization studies, where the so-called ''binary encounter peak'' is due to the elastic scattering of a quasi-free-electron in a neutral target from the projectile ion (see, for example, Ref. [10] and references therein). The interpretation of the DCS is complicated, however, by the effect of the host atom on the quasi-free-electron.

The measurements [2–9] and calculations for various ions [1,11–15] apply, strictly, only to systems where the electron scatters elastically at energies well below the first inelastic threshold. In the above-mentioned applications, however, the energies of the incident electrons are frequently sufficient to produce an excited state of the target ion, and so, as discussed in Sec. III, the electron-ion interaction may be complicated by inelastic absorption processes and the formation of elastic resonances. For further simplicity, there is a tendency in both experiment and theory to consider only closed-shell ions, since it is then unnecessary to account for the coupling between the orbital angular momenta and spin of the incident electron and those of the target ion (see Sec. III B). We therefore investigate a more challenging problem, where an electron scatters elastically from an open-shell ion at an energy above the first inelastic threshold.

As the charge of the ion for a given nucleus increases, measurements [8] and partial wave calculations [16] show

*Present address: Department of Physics and Astronomy, University of Glasgow, Glasgow G12 8QQ, UK.

that the DCS approaches the Rutherford form. To obtain the most accurate information about the short-range electron-ion interaction, we therefore study a singly charged ion. The Ar^+ system is one of the most interesting of the singly charged ions, since, due to a low-energy shape resonance, there is the largest rise in the *d*-wave phase shift as the collision energy increases [11]. The *d*-wave phase shift for Ar^+ is consequently especially sensitive to the scattering potential used in the calculations and, hence, the inclusion of coupling and relaxation effects (see Sec. III) and the accurate representation of polarization become more important.

In view of the above discussion, we present below the measured DCS for the elastic scattering of electrons from $Ar^+(3s^2 3p^5\ ^2P)$ at an energy above one inelastic threshold and, by solving the Hartree-Fock equations, calculate the corresponding theoretical DCS including the coupling and relaxation effects. To determine the importance of accurately representing the scattering potential when modeling electron-ion collisions, we compare the measurements with our calculation and an uncoupled, unrelaxed theory. Finally, by fitting to the measurements, we obtain the non-Coulomb phase shifts for comparison with the calculations of Manson and Turner [14].

II. EXPERIMENTAL DETAILS

The electron spectrometer is described in other publications [5,6,17,18], and so only a brief discussion is given here. The Ar^+ beam produced by a 5 GHz electron cyclotron resonance (ECR) ion source [19,20] is transported to the interaction region, where it is decelerated to 1 keV with a typical current of 1 μA and focused to a spot diameter of 3 mm. The electrostatically confined gun lens system is based on a design described by Bernius, Man, and Chutjian [21] that produces a near parallel (see below) 1 mm beam of electrons with a current and energy resolution [full width at half maximum (FWHM)] of 150 nA and 0.6 eV, respectively, which intersects the target ion beam at 90°. The energies of the electrons scattered from the interaction region are measured by an electrostatic hemispherical deflection analyzer, which uses two triple aperture electrostatic lenses and is similar to a design discussed by Brunt, Read, and King [22]. To observe at different scattering angles, the analyzer can be rotated between $-20°$ and 85° with respect to the direction of the incident electron beam. The energy analyzed image at the exit plane of the analyzer is recorded by a position sensitive detector. The corrections for the transformation from the laboratory to the center of mass reference frame at less than 0.013 eV and 0.1° for the collision energy and scattering angle, respectively, in the angular range studied are negligible. The base pressure in the interaction chamber is 5×10^{-10} mbar.

The density of ions in the beam at 10^5 cm^{-3} is very low compared to the typical values of 10^{12} to 10^{14} cm^{-3} for a neutral gas target. Therefore, most of the counts recorded are due to electrons scattering elastically from nontarget, residual gas in the chamber or metallic surfaces, and this yield will be referred to as the background. The ion beam is consequently switched on (giving the Ar^+ plus background counts) and off (yielding the background counts only) to allow the target ion signal to be separated from the background noise. The space-charge potential across the ion beam can deflect the incident and scattered electrons. It is therefore important to ensure that the electron beam is parallel rather than sharply focussed, for otherwise the degree of deflection can be significant. The background counts would then be measured at a different scattering angle than the target ion plus background counts, which could lead to an inaccurate estimate of the Ar^+ signal.

Ion beams produced by different electron impact sources usually contain some fraction of metastable states (see Hofer *et al.* [23] for Ar^+, Kr^+, and Xe^+). Using the energy levels of Ar^+ (Griffin *et al.* [24] and references therein), we expect that the ground-state beam contains metastable states such as $3p^4(^3P)3d\ ^4D_{7/2}$ (see Varga, Hofer, and Winter [25] for a fuller list of the metastable states and discussion). The ECR source was tuned to maximize the production of singly ionized Ar, and so the fraction of ions in more highly charged states is relatively small. The metastable states are therefore mainly produced in single collisions, that is, by a direct transition or after cascading from more highly excited states of Ar^+, rather than from electron capture into states of higher charge. The measurements of Ref. [25] for single collision conditions can consequently be used, which show that the metastable fraction in a singly charged Ar beam is less than 4% for all energies of the incident ionizing electrons. We therefore expect that metastable states do not produce significant effects in the measurements presented below.

III. THEORY FOR SCATTERING BY A MODIFIED COULOMB POTENTIAL

In Sec. III A, we begin by discussing the simplest systems, namely, where an electron scatters elastically from a closed-shell ion at energies well below the first inelastic threshold. The physical complications arising when the incident electron has sufficient energy to excite a state of the target or the ion is open shelled are discussed in Secs. III B to III D.

L-S coupling is used below, where the approximation is made that the total orbital angular momentum *L* and the total spin *S* are conserved separately in the scattering process. The calculations of Johnson and Guet [1] for Cs^+ show that the spin-flip cross section is small. Since spin-orbit effects increase as approximately the second power of the nuclear charge *Z* for low-charged many-electron ions, we expect that *L-S* coupling is accurate for the lighter ion Ar^+.

A. Elastic scattering from a closed-shell ion below the first inelastic threshold

For electron-ion collisions, the scattering potential is of the Coulomb form at large distances *r* between the scattered electron and the ion, but departs from a $1/r$ dependence at smaller distances where the charge density of the target is significant. The potential is therefore written as

$$V(r) = V_s(r) - \frac{Z_i}{r}, \tag{1}$$

where $V_s(r)$ is the *spherically symmetric*, short-range potential; Z_i is the charge of the target ion; and atomic units are used in this section. Due to the short-range potential, there is an additional phase shift σ_l relative to the Coulomb phase shift δ_l, and so the scattering amplitude becomes

$$f_{\rm el}(\theta)=\frac{1}{2ik}\sum_{l=0}^{\infty}(2l+1)[e^{2i(\delta_l+\sigma_l)}-1]P_l(\cos\theta), \quad (2)$$

where k is the wave number, l is the orbital angular momentum quantum number, and θ is the scattering angle. The Coulomb phase shifts δ_l are calculated using

$$\delta_l=\arg\Gamma(l+1-iZ_i/k). \quad (3)$$

In contrast to most scattering problems where only the first few partial waves l are significant, Eq. (3) shows that the partial wave decomposition of the Coulomb scattering amplitude

$$f_c(\theta)=\frac{Z_i}{2k^2\sin^2(\theta/2)}\exp\{i(Z_i/k)\ln[\sin^2(\theta/2)]+2i\delta_0\} \quad (4)$$

requires an infinite number of angular momenta l. To avoid the summation from $l=0$ to infinity in Eq. (2), it is therefore mathematically convenient to separate $f_{\rm el}(\theta)$ into a Coulomb term $f_c(\theta)$ and a term due to the short-range potential $f_s(\theta)$ by writing (see pp. 65 and 66 in Ref. [26] for further details)

$$f_{\rm el}(\theta)=f_c(\theta)+f_s(\theta), \quad (5)$$

where

$$f_s(\theta)=\frac{1}{2ik}\sum_{l=0}^{\infty}(2l+1)e^{2i\delta_l}[e^{2i\sigma_l}-1]P_l(\cos\theta). \quad (6)$$

The non-Coulomb phase shifts approach zero with increasing l in such a way that the partial wave expansion of $f_s(\theta)$ converges rapidly. The differential cross section is then given by

$$\frac{d\sigma}{d\Omega}=|f_c(\theta)+f_s(\theta)|^2=|f_c(\theta)|^2+|f_s(\theta)|^2 + 2\,\mathrm{Re}\{f_c^*(\theta)f_s(\theta)\}. \quad (7)$$

The non-Coulomb phase shifts for all net charges of a positive ion in its ground state with the nuclear charge Z have been calculated by Manson and Turner [14] for $2\leqslant Z\leqslant 30$. The spherically symmetric, Herman-Skillman (Hartree-Slater) potential [11] was used:

$$V(r)=-\frac{Z}{r}+\frac{1}{r}\int_0^r\alpha(t)dt+\int_r^{\infty}\frac{\alpha(t)}{t}dt-3\left(\frac{3}{8\pi}\rho(r)\right)^{1/3}, \quad (8)$$

where $\rho(r)=\alpha(r)/4\pi r^2$ is the spherically averaged total electronic charge density of the ion calculated using the wave function of neutral Ar with one $3p$ electron removed. The approximation is made that the removal of the $3p$ electron does not produce a redistribution of charge in the residual ion, and so the charge density $\rho(r)$ and the corresponding scattering potential $V(r)$ are referred to as unrelaxed or ''frozen.'' The last term on the right-hand side of Eq. (8), proportional to the one-third power of the electronic density, is a *local* potential that gives an approximate representation of the effects of exchange averaged over the total spin states S [12]. The calculation using Eqs. (4)–(7) and the non-Coulomb phase shifts by Manson and Turner [14] is referred to below as the Herman-Skillman (HS) method, and the resulting DCS will be compared with experiment in Sec. IV. The phase shifts for $l=0$, 1, and 2 have also been computed by Szydlik, Kutcher, and Green [12] using the independent particle model potentials of Green, Sellin, and Zachor [27].

B. Elastic scattering from an open-shell ion

For the present open-shell target, the orbital angular momentum l of the incident electron and that of the ion, ^2P, couple to form the total orbital angular momentum L, which for $l\geqslant 1$ gives $L=l-1$, l, and $l+1$, and the spins couple to form a singlet or triplet state. To account for the orbital angular momentum of the ion requires a spherically asymmetric potential, and to formally include the coupling between the spins necessitates the use of a nonlocal exchange potential (see, for example, Ref. [28]). In Sec. III A, however, the target ion is represented by a Coulomb field plus a *local, spherically symmetric* potential. To account for the coupling effects, we therefore calculated the phase shifts by solving the Hartree-Fock equations for each partial wave l of the incident electron in the self-consistent field of Ar^+ $(3s^2 3p^5\ ^2P)$. In the present approach, the Hartree-Fock potential depends on the total orbital angular momentum L and the total spin S using a nonlocal exchange potential. Furthermore, the self-consistent field of the ground state of Ar^+ includes the effects of relaxation. Our phase shifts for the first six partial waves l and the allowed L and S are shown in Table I. In the expression for the scattering amplitude $f_s(\theta)$, the terms within the summation must be weighted by the appropriate factors, that is,

$$f_{\rm el}^{\pm}(\theta)=f_c(\theta)+\frac{1}{2ik}\left[e^{2i\delta_0}(e^{2i\sigma_0^{\pm}}-1)+\sum_{l=1}^{\infty}\sum_{L=l-1}^{l+1}\frac{(2L+1)}{3}e^{2i\delta_l}(e^{2i\sigma_{lL}^{\pm}}-1)P_l(\cos\theta)\right], \quad (9)$$

TABLE I. The non-Coulomb phase shifts $\sigma_{lL}(S)$ for the elastic scattering of electrons from $Ar^+(3s^2 3p^5\ ^2P)$ at the collision energy of 16 eV calculated using the coupled HF method.

l	L	σ_{lL} $(S=0)$	σ_{lL} $(S=1)$
0	1	6.097 931	6.183 35
1	0	4.105 193	4.731 643
1	1	4.475 451	4.475 451
1	2	4.504 555	4.577 443
2	1	0.373 763	1.744 557
2	2	1.443 881	1.443 881
2	3	1.464 724	1.642 101
3	2	0.071 966	0.183 89
3	3	0.040 775	0.040 775
3	4	0.113 467	0.145 724
4	3	0.031 656	0.043 514
4	4	−0.028 238	−0.028 238
4	5	0.024 367	0.028 62
5	4	0.017 445	0.018 876
5	5	−0.025 17	−0.02 517
5	6	0.010 753	0.011 357

where the superscripts + or − denote singlet or triplet scattering, respectively. In our experiment the average over the four possible spin states is observed, and so the differential cross section is given by

$$\frac{d\sigma_{\rm av}}{d\Omega}=\frac{1}{4}|f_{\rm el}^{+}|^2+\frac{3}{4}|f_{\rm el}^{-}|^2. \tag{10}$$

The singlet, triplet, and spin-averaged differential cross sections calculated using the phase shifts in Table I and Eqs. (9) and (10) are shown in Fig. 1.

To determine the importance of including relaxation, we calculated the unrelaxed phase shifts using the ''frozen'' field of the neutral Ar atom with one $3p$ electron removed. The relaxation was found to cause the non-Coulomb phase shifts to reduce, especially for the d wave where the decrease after averaging over L and S is 0.20 rad. The σ_l reduce because the electron cloud for the relaxed ground state of Ar^+ is slightly less diffuse and, hence, the attraction by the potential is smaller.

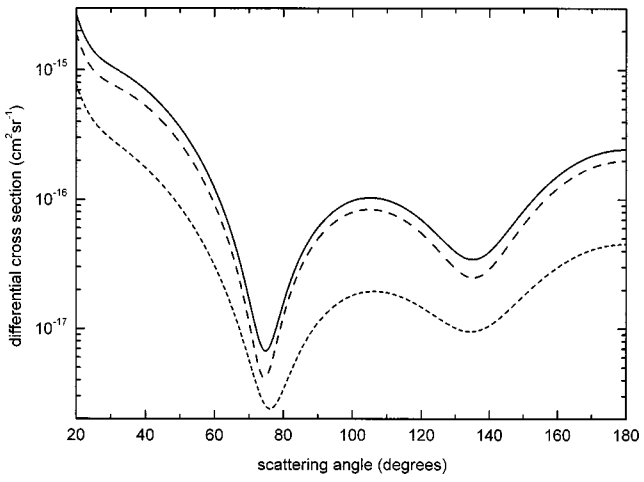

FIG. 1. The singlet (short-dashed curve), triplet (long-dashed curve), and spin-averaged (solid curve) differential cross sections for the elastic scattering of electrons from $Ar^+(3s^2 3p^5\ ^2P)$ at the collision energy of 16 eV calculated using the coupled HF method.

C. Inelastic processes

The method of partial waves with *real* phase shifts discussed in Secs. III A and III B applies only to elastic collisions. However, the impact energy in the experiment at 16 eV lies above one inelastic threshold due to the transition $3s^2 3p^5\ ^2P-3s3p^6\ ^2S$, which requires the excitation energy of 13.48 eV [29]. To account for the resulting absorption from the incident beam, it is a standard practice to introduce complex phase shifts,

$$\sigma_l(k)=\mathrm{Re}\,\sigma_l(k)+i\,\mathrm{Im}\,\sigma_l(k). \tag{11}$$

For the present purposes, it is sufficient to use the uncoupled formula (5) rather than the coupled expression (9). The scattering amplitude for a modified Coulomb potential at energies above the first inelastic threshold then becomes

$$f_{\rm el}(\theta)=f_c(\theta)+\frac{1}{2ik}\sum_{l=0}^{\infty}(2l+1)e^{2i\delta_l}\times[\eta_l(k)e^{2i\,\mathrm{Re}\,\sigma_l}-1]P_l(\cos\theta), \tag{12}$$

where $\eta_l(k)$ is the absorption factor defined by

$$\eta_l(k)=\exp[-2\,\mathrm{Im}\,\sigma_l(k)]. \tag{13}$$

To determine the effect of the inelastic process on the elastic DCS, we therefore require the absorption factors $\eta_l(k)$ for each significant partial wave l. The $\eta_l(k)$ are related to the partial inelastic cross sections $\sigma_l^{\rm abs}$ by

$$\sigma_l^{\rm abs}=\frac{\pi}{k^2}(2l+1)(1-\eta_l^2). \tag{14}$$

However, although the total inelastic cross section $\sigma_{\rm abs}$ has been calculated by Tayal and Henry [30], it appears that the partial cross sections $\sigma_l^{\rm abs}$ are unavailable in the literature. We might consequently, instead, consider estimating the relative importance of the inelastic process by comparing $\sigma_{\rm abs}$ with the total elastic cross section $\sigma_{\rm el}$ but $\sigma_{\rm el}$ is infinite. We therefore first make the approximation that the DCS for the inelastic process is isotropic. Using the following value for the total inelastic cross section at the collision energy of 16 eV [30]:

$$\sigma_{\rm abs}=3.28\times10^{-17}\ \mathrm{cm}^2, \tag{15}$$

the ratio of the inelastic DCS to that for elastic scattering from a Coulomb potential, $|f_c(\theta)|^2$, is then given approximately by

$$\frac{d\sigma_{\rm abs}}{d\Omega}\Big/\frac{d\sigma_{\rm el}}{d\Omega}\approx\frac{\sigma_{\rm abs}}{4\pi}\Big/|f_c(\theta)|^2=0.5\sin^4(\theta/2), \tag{16}$$

which is negligibly small over most of the angular range observed and reaches a maximum of 0.1 at 85°. We therefore do not include the effects of the inelastic process in the analysis of Sec. IV. The neglect of the complex phase shifts is supported by the elastic scattering of electrons from the neutral gases Ar, Kr, and Xe, where it is found that the complex potential has little effect on the DCS even at energies well above the first inelastic thresholds [31].

D. Elastic resonances

The elastic resonances are produced by the doubly excited states of neutral argon, which occur when the incident electron is temporarily trapped in the attractive field provided by an excited state of the ion. The doubly excited states so populated can decay to the initial ground state Ar^+ $(3s^2 3p^5\ ^2P)$ or the excited state Ar^+ $(3s3p^6\ ^2S)$, which are referred to as the elastic and inelastic channels, respectively. Tayal and Henry [30] calculated the collision strengths for the transition $3s^2 3p^5\ ^2P - 3s3p^6\ ^2S$ as a function of the impact energy, which shows that the resonances cover the energy range of the present experiment. We therefore consider below the effects of such resonances on the elastic DCS.

In this section, for simplicity, we use the uncoupled [Eq. (5)] rather than the coupled expression [Eq. (9)] for the scattering amplitude. The elastic scattering amplitude when one or more partial waves l' are resonant then becomes (similar expressions without the Coulomb phase shifts are derived in pp. 604–607 of Ref. [32] and Appendix C in Ref. [33])

$$f_{\rm el}(\theta) = f_c(\theta) + f_s(\theta) - \sum_{l'} \frac{(2l'+1)}{2k} \frac{\Gamma_{\rm el} e^{2i(\delta_{l'}+\sigma_{l'})} \eta_{l'}}{E - E_r + i\Gamma/2} P_{l'}(\cos\theta), \tag{17}$$

where $f_c(\theta)$ and $f_s(\theta)$ are defined in Sec. III A, E_r is the resonance energy, and the total width Γ is given by

$$\Gamma = \Gamma_{\rm el} + \Gamma_{\rm in}, \tag{18}$$

with $\Gamma_{\rm el}$ and $\Gamma_{\rm in}$ denoting the partial widths for the decay to the elastic and inelastic channels, respectively. The doubly excited states decay predominantly to the elastic channel, and therefore, to a good approximation, $\Gamma_{\rm el}$ can be replaced by Γ in Eq. (17). To the best of our knowledge the resonance parameters required to calculate the elastic DCS using Eq. (17) are unavailable, namely, the energies E_r, widths Γ, and classifications L^π of the doubly excited states of neutral argon in the energy range of our experiment. The classifications of the doubly excited states are needed to determine which partial waves l' can couple to the ground state of the ion, P^o, to form the given L^π and, hence, are resonant.

Figure 1 in Ref. [30] shows that there is a broad resonance centered at the collision energy of approximately 16 eV. To investigate the effect of such a doubly excited state without knowledge of the resonance parameters, we calculated the elastic DCS for many different resonance energies, widths, and classifications. As an example, we show in Fig. 2 the theoretical DCS including a F^o doubly excited state that couples to the d and g partial waves. In Fig. 2, the non-Coulomb phase shifts are set equal to the values of Manson and Turner [14] as shown in Table II; the resonance energy E_r is put at the impact energy E to display the maximum possible effect of the doubly excited state; and we use 50 meV as an estimate for Γ, since this value is typical of the widths for the lower lying doubly excited states $3s3p^6 ns$, np, and nd of argon in the energy range of 9.2 to 12.5 eV (relative to the ground state of Ar^+) measured by Mitchell *et al.* [34]. To account for the imperfect energy resolution of the spectrometer, we show in Fig. 2 the theoretical curve including the F^o resonance convolved with a Gaussian apparatus function of 0.6 eV FWHM and, for comparison, the angular distribution without the resonance or convolution is included. Clearly, the effect of a doubly excited state, although potentially large for perfect energy resolution (FWHM=0), is significantly reduced when observed in the present experiment. Furthermore, the reduction in the influ-

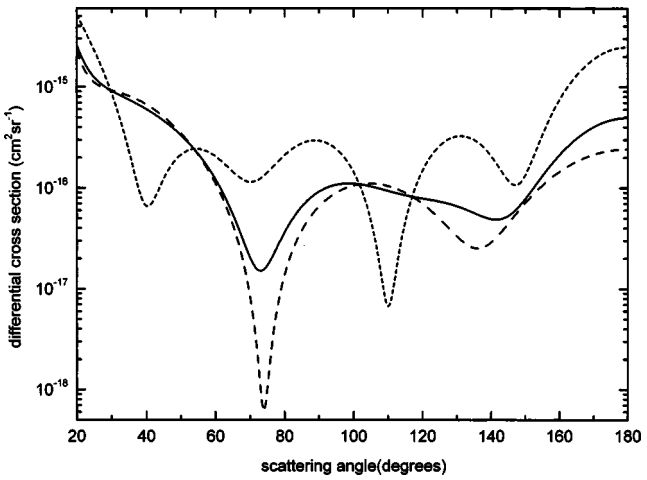

FIG. 2. The theoretical differential cross section including an F^o elastic resonance observed with perfect energy resolution (short-dashed curve) and a Gaussian apparatus function of 0.6 eV full width at half maximum (solid curve). For comparison, the angular distribution without a resonance or convolution is included (long-dashed curve).

TABLE II. The calculated non-Coulomb phase shifts σ_l of Ref. [14] compared to the values obtained by least-squares fitting to the measurements and the corresponding χ^2. The coupled phase shifts $\sigma_{lL}(S)$ (see Table I) averaged over the total spin S and the total orbital angular momentum L weighted by the factors $(2S+1)(2L+1)$ are included.

	Ref. [14]	Least squares	Average
σ_0	6.172	6.34±0.17	6.161
σ_1	4.575	4.26±0.14	4.533
σ_2	1.714	1.686±0.085	1.507
σ_3	0.0699	0.0699	0.110
σ_4	0.004 25	0.004 25	0.0123
σ_5	0.000 34	0.000 34	0.001 07
χ^2	49.53	36.08	

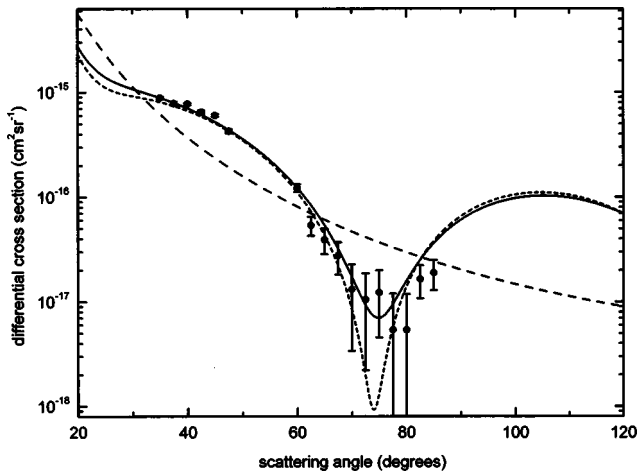

FIG. 3. Comparison between the measured differential cross section (circles), the HS calculation (short-dashed curve), the coupled HF calculation (solid curve), and the Rutherford cross section (long-dashed curve).

ence of the resonance is greater or smaller depending on whether the width Γ is narrower or broader than 50 meV, respectively. For perfect energy resolution, the effect of a doubly excited state is only to add a constant phase shift to $\sigma_{l'}$ for each resonant partial wave l', and so the DCS can still be parametrized by equations of the type (4)–(6).

IV. THE COMPARISON BETWEEN EXPERIMENT AND THEORY

In Fig. 3, the measured DCS for the elastic scattering of electrons from Ar^+ $(3s^2 3p^5\ ^2P)$ at the collision energy of 16 eV is compared to the HS method (see Sec. III A), the coupled HF approach (see Sec. III B), and the Rutherford cross section. The experimental data are normalized to the coupled HF theory at the scattering angle of 35°. The error bars represent the statistical reproducibility of the data at the 90% confidence level and include the effect of subtracting the background (see Sec. II). To account for the angular acceptance of the electron analyzer, each theoretical DCS in Fig. 3 is shown convolved with a Gaussian function G of 2° FWHM, that is,

$$I(\theta)=\int_0^{180}\frac{d\sigma(\theta_0)}{d\Omega}G(\theta-\theta_0)d\theta_0. \tag{19}$$

The angular broadening causes a small reduction in the depth of the minima centered at approximately 75°, and the sharper the minimum the greater the reduction. The measurements deviate significantly from the Rutherford cross section over the full angular range observed, especially in the region of a deep minimum centered at approximately 75°. Both calculations reproduce the overall shape of the measured DCS, although the coupled HF approach describes the depth of the minimum more accurately.

To understand why the minimum is shallower in the coupled HF method, we averaged the coupled phase shifts over the total spin S and the total orbital angular momentum L weighted by the factors $(2S+1)(2L+1)$. The average values are compared to the phase shifts of Manson and Turner [14] in Table II, which shows that the σ_l are similar with the important exception of σ_2. The coupled HF method therefore describes the depth of the measured minimum more accurately due, mainly, to the lower average value for the *d*-wave phase shift. If a resonant state is present, however, then a shallower minimum could be produced using the phase shifts of Manson and Turner [14], as discussed in Sec. III D and illustrated in Fig. 2 for a particular L^π.

In the HS and coupled HF methods, we consider next why only the σ_2 differ significantly. For *d*-wave scattering from Ar^+, the potential consists of a double well separated by a barrier [35,36]. The behavior of σ_2 is therefore atypical for the following two reasons [11–13,37]. First, the *d* wave starts to penetrate into the inner potential well as the collision energy increases from 0 to approximately 2 Ry, which causes σ_2 to rise rapidly. Due to the resulting low-energy *d*-wave shape resonance, σ_2 is more sensitive to the details of the potential used in the calculations. A similar atypical behavior occurs for *f*-wave scattering from Cs^+ [1,13]. To understand the second reason, consider the ''effective potential'' or the sum of the attractive electrostatic and repulsive centrifugal potentials. Owing to the partial cancellation between the electrostatic and centrifugal terms in the region of the double well, the effective potential is very much smaller than the electrostatic or centrifugal potentials individually. Consequently, small changes in the electrostatic potential cause large relative changes in the effective potential. Thus, the double well and barrier leads to an increased sensitivity even when the resonant trapping of the wave function in the inner potential well becomes small, which explains the difference of approximately 0.2 rad between the σ_2 at energies well above the *d*-wave resonance. A related discussion comparing the HS and HF phase shifts for the photoionization of neutral Ar is given by Kennedy and Manson [38]. In summary, we suggest that the significant separation between the σ_2 is due to the high sensitivity of the *d*-wave phase shift to the different scattering potentials used in the HS and coupled HF methods. In particular, as discussed in Secs. III A and III B, the use of a relaxed potential here rather than the unrelaxed potential in Ref. [14] is the main cause of our lower average value for σ_2.

To obtain the non-Coulomb phase shifts accounting for the angular acceptance of the electron analyzer, we least-squares fitted the convolved expression (19) for the DCS to the measurements using the Levenberg-Marquardt method [39]. The three terms on the right-hand side of Eq. (9) for each partial wave l with different total angular momenta $L=l-1$, l, and $l+1$ have the same angular dependence, and the resulting degeneracy makes it impossible to fit to our measurements using the coupled formula. We therefore optimized the uncoupled expression (see Sec. III A) in which all the terms, by contrast to Eq. (9), are orthogonal when integrated over the scattering angle. In view of the limited angular range observed and the statistical uncertainties involved, only the *s*, *p*, and *d* non-Coulomb phase shifts were optimized whilst σ_3, σ_4, and σ_5 were fixed at the theoretical values of Ref. [14]. Due to the large angular momentum

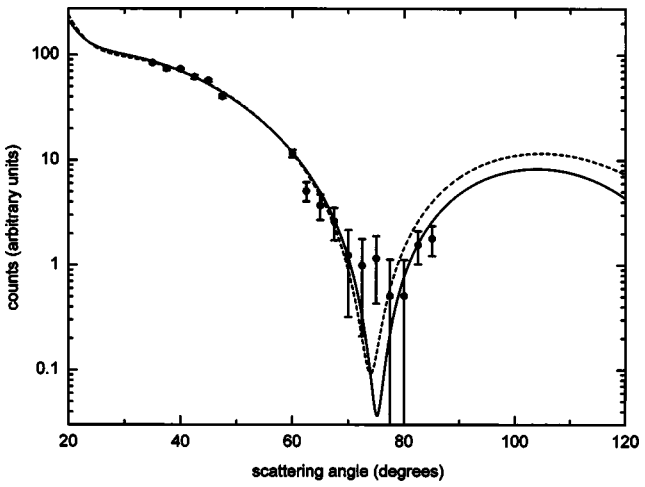

FIG. 4. The fit (solid curve) to the measurements (circles) and the differential cross section calculated using the phase shifts of Ref. [14] (dashed curve).

barrier for $l \geqslant 3$, all the calculations (Refs. [11], [14], and the present coupled HF) show that the phase shifts $\sigma_{l \geqslant 3}$ are small ($\lesssim 0.1$ rad) and, hence, have only a slight effect on the DCS. Therefore, fixing σ_3, σ_4, and σ_5 to theory has only a very small effect on the fitted values of σ_0, σ_1, and σ_2. The optimized non-Coulomb phase shifts are presented in Table II and the corresponding fitted DCS is shown in Fig. 4. The DCS according to the HS method is included in Fig. 4, which has been convolved with a Gaussian function to account for the angular acceptance of the electron analyzer [see Eq. (19)]. For the nonlinear parameters σ_l, the errors ε_l in Table II are defined by [40]

$$\chi^2(\sigma_{lm}+\varepsilon_l)=\chi^2(\sigma_{lm})+1 \tag{20}$$

and account for the statistical uncertainties, where σ_{lm} is the value of σ_l that gives the minimum χ^2. When using Eq. (20) to determine $\sigma_{\overline{lm}}$ for a particular partial wave $\overline{l}$, the non-Coulomb phase shifts σ_{lm} for all the other partial waves ($l < 3$) are reoptimized, and therefore the resulting error estimate also accounts for the correlation between the phase shifts or the nonuniqueness of the fitting procedure. In addition, there are probably also small nonstatistical errors, such as those caused by removing the background as discussed in Sec. II, which are difficult to estimate and so are not included in the ε_l. The χ^2 obtained when all the σ_l are fixed at the values of Manson and Turner [14] is included in Table II, which confirms the expectation that the agreement with experiment improves by optimizing the first three non-Coulomb phase shifts. The number of degrees of freedom ν for the present analysis is 13, and so for good fits χ^2 is approximately normally distributed with a mean value of 13 and a standard deviation $\sqrt{2\nu}$ of 5.1 [40]. The value of χ^2 obtained here at 36.1 therefore suggests that the model and the data are not quite consistent within the quoted experimental uncertainties, which is probably due to small nonstatistical errors (see above). Similarly, values of χ^2 significantly larger than the number of degrees of freedom are also obtained when fitting the phase shifts to other electron-ion elastic scattering measurements [41]. Table II shows that the *s* and *d* non-Coulomb phase shifts according to Manson and Turner [14] and the fit are consistent within the quoted experimental uncertainties, although there is possibly a small discrepancy for the *p* wave. The fitted σ_2 is closer to the value of Manson and Turner [14] than the coupled HF result, which seems to contradict the observation that the lower *d*-wave phase shift describes the depth of the measured minimum more accurately. However, we suspect that the fitting procedure is compensating for a small systematic error due to a data point or points away from the minimum at approximately 75°, which otherwise would give a value of σ_2 closer to 1.507.

The distortion of the ion by the incident electron during the collision alters the scattering potential, but the resulting polarization effects are not included in the present static-exchange method. The agreement between our measurements and calculation suggests, however, that the effect of polarization on the phase shifts is small ($\lesssim 0.1$ rad).

V. CONCLUSION

Measurements of the DCS for the elastic scattering of electrons from $Ar^+(3s^2 3p^5\ ^2P)$ at the collision energy of 16 eV have been presented. We calculated the corresponding non-Coulomb phase shifts σ_l by solving the Hartree-Fock equations for the incident electron in the self-consistent field of $Ar^+(3s^2 3p^5\ ^2P)$. The coupling between the orbital angular momenta and spin of the incident electron and those of the target ion are formally included in our model, since the Hartree-Fock potential here depends on the total orbital angular momentum L and the total spin S using a nonlocal exchange potential. Furthermore, the self-consistent field of the ground state of Ar^+ includes the effects of relaxation. We compared the measurements with our coupled HF calculation and an uncoupled, unrelaxed theory using a local, spherically symmetric HS potential. Both calculations reproduce the overall deviations of the experimental data from the Rutherford cross section, but the coupled HF approach describes the depth of the measured minimum at around 75° more accurately owing to our lower average value for σ_2.

For *d*-wave scattering from Ar^+, the potential consists of a double well separated by a barrier. Consequently, there is a *d*-wave shape resonance and small changes in the electrostatic potential cause large relative changes in the effective potential (electrostatic plus centrifugal terms). Therefore, the *d*-wave phase shift is highly sensitive to the details of the scattering potential used in the calculations, which explains why only the σ_2 differ significantly in the HS and coupled HF methods. In particular, the use of a relaxed rather than an unrelaxed potential here is the main cause of our lower σ_2. Thus, we have shown that the experimental DCS for electron-ion collisions in the energy range of a shape resonance provides a stringent test of the accuracy of the approximations of the theory.

The DCS is dominated by the Rutherford cross section at low scattering angles. To obtain the most accurate information about the short-range electron-ion interaction, the angular distribution at larger scattering angles is consequently re-

quired, particularly in the backward hemisphere ($90° < \theta \leqslant 180°$). We therefore intend to modify the present apparatus to allow observations over the full angular range ($0° \leqslant \theta \leqslant 180°$). The detailed structure expected at larger scattering angles would permit phase shifts to be fitted with greater accuracy and the optimization of higher partial waves. The resulting σ_l would test more stringently the approximations of the calculations and thereby advance our understanding of electron-ion interactions.

ACKNOWLEDGMENT

We thank Professor S. T. Manson for comments on the manuscript.

[1] W. R. Johnson and C. Guet, Phys. Rev. A **49**, 1041 (1994).
[2] B. A. Huber, C. Ristori, C. Guet, D. Küchler, and W. R. Johnson, Phys. Rev. Lett. **73**, 2301 (1994).
[3] J. B. Greenwood, I. D. Williams, and P. McGuinness, Phys. Rev. Lett. **75**, 1062 (1995).
[4] I. D. Williams, in *Proceedings of the 20th International Conference on Physics of Electronic and Atomic Collisions*, Vienna, edited by F. Aumayr and H. Winter (World Scientific, Singapore, 1998), p. 313.
[5] B. Srigengan, I. D. Williams, and W. R. Newell, Phys. Rev. A **54**, R2540 (1996).
[6] B. Srigengan, I. D. Williams, and W. R. Newell, J. Phys. B **29**, L897 (1996).
[7] C. Belenger, P. Defrance, R. Friedlein, C. Guet, D. Jalabert, M. Maurel, C. Ristori, J. C. Rocco, and B. A. Huber, J. Phys. B **29**, 4443 (1996).
[8] I. D. Williams, B. Srigengan, J. B. Greenwood, W. R. Newell, A. Platzer, and L. O'Hagan, Phys. Scr. T **73**, 119 (1997).
[9] Z. Wang, J. Matsumoto, H. Tanuma, A. Danjo, M. Yoshino, and N. Kobayashi, J. Phys. B **33**, 2629 (2000).
[10] C. Liao, S. Hagmann, C. P. Bhalla, S. R. Grabbe, C. L. Cocke, and P. Richard, Phys. Rev. A **59**, 2773 (1999).
[11] S. T. Manson, Phys. Rev. **182**, 97 (1969).
[12] P. P. Szydlik, G. J. Kutcher, and A. E. S. Green, Phys. Rev. A **10**, 1623 (1974).
[13] D. C. Griffin and M. S. Pindzola, Phys. Rev. A **53**, 1915 (1996).
[14] S. T. Manson and C. S. Turner (private communication).
[15] J. T. Shepherd and A. S. Dickinson, J. Phys. B **32**, 513 (1999).
[16] I. D. Williams, Rep. Prog. Phys. **62**, 1 (1999).
[17] B. Srigengan, I. D. Williams, and W. R. Newell, J. Phys. B **29**, L605 (1996).
[18] P. McKenna, B. Srigengan, and I. D. Williams (unpublished).
[19] M. Liehr, G. Mank, and E. Salzborn, NSCL Report No. MSUCP-47, 1987 (unpublished).
[20] T. K. McLaughlin, Ph.D. thesis, Queen's University of Belfast, 1992 (unpublished).
[21] M. T. Bernius, K. F. Man, and A. Chutjian, Rev. Sci. Instrum. **59**, 2418 (1988).
[22] J. N. Brunt, F. H. Read, and G. C. King, J. Phys. E **10**, 134 (1977).
[23] W. Hofer, W. Vanek, P. Varga, and H. Winter, Rev. Sci. Instrum. **54**, 150 (1983).
[24] D. C. Griffin, M. S. Pindzola, J. A. Shaw, N. R. Badnell, M. O'Mullane, and H. P. Summers, J. Phys. B **30**, 3543 (1997).
[25] P. Varga, W. Hofer, and H. Winter, J. Phys. B **14**, 1341 (1981).
[26] N. F. Mott and H. S. W. Massey, *The Theory of Atomic Collisions*, 3rd ed. (Oxford University Press, London, 1965).
[27] A. E. S. Green, D. L. Sellin, and A. S. Zachor, Phys. Rev. **184**, 1 (1969).
[28] B. H. Bransden and C. J. Joachain, *Physics of Atoms and Molecules* (Longman, Harlow, 1983), Sec. 12.2.
[29] C. E. Moore, *Atomic Energy Levels*, Natl. Stand. Ref. Data Ser., Natl. Bur. Stand. (U.S.) Circ. No. 35 (U.S. GPO, Washington, D.C., 1971), Vol. 1.
[30] S. S. Tayal and R. J. W. Henry, J. Phys. B **29**, 3443 (1996).
[31] R. A. Berg, J. E. Purcell, and A. E. S. Green, Phys. Rev. A **3**, 508 (1971).
[32] H. S. W. Massey and E. H. S. Burhop, *Electronic and Ionic Impact Phenomena*, 2nd ed. (Oxford University Press, London, 1969), Vol. 1.
[33] U. Fano, Phys. Rev. **124**, 1866 (1961).
[34] P. Mitchell, J. A. Baxter, J. Comer, and P. J. Hicks, J. Phys. B **13**, 4481 (1980).
[35] A. R. P. Rau and U. Fano, Phys. Rev. **167**, 7 (1968).
[36] S. T. Manson and J. W. Cooper, Phys. Rev. **165**, 126 (1968).
[37] S. M. Younger, Phys. Rev. A **26**, 3177 (1982).
[38] D. J. Kennedy and S. T. Manson, Phys. Rev. A **5**, 227 (1972).
[39] D. W. Marquardt, J. Soc. Ind. Appl. Math. **11**, 431 (1963).
[40] P. R. Bevington, *Data Reduction and Error Analysis for the Physical Sciences* (McGraw-Hill, New York, 1969).
[41] M. C. Per and A. S. Dickinson, J. Phys. B **33**, 3485 (2000).